Electronic Supplementary Information

Experimental section

Materials: Copper foam (CF) with high purity was provided by Tianjin Gaossunion Photoelectric Technology Co., Ltd. Sulfanilamide was purchased from Shanghai Macklin Biochemical Technology Co., Ltd. $C_{12}H_{14}N_2 \cdot 2HCl$ was purchased from Shanghai J&K Scientific Technology Co., Ltd. Salicylic acid, urea, sodium citrate, $C_5FeN_6Na_2O \cdot 2H_2O$, $Co(NO_3)_2 \cdot 6H_2O$, H_3PO_4, NaOH, NH_4Cl, and $NaNO_3$ were purchased from Shanghai Aladdin Reagent Co., Ltd. C_2H_5OH, HNO_3, HCl, and NaClO were obtained from Chengdu Kelon Chemicals Co., Ltd. Ultrapure H_2O with a resistivity of 18 MΩ·cm^{-1} was used throughout the experiments.

Synthesis of CoF$_2$ NS/CF: CF was cleaned ultrasonically using deionized water and absolute ethyl alcohol followed by drying in an oven at 60°C. CoF_2 NS/CF was prepared in two steps. First, 2 mmol of $Co(NO_3)_2 \cdot 6H_2O$ and 10 mmol of $CO(NH_2)_2$ were dissolved in 35 mL of H_2O. Subsequently, the resulting solution was transferred into a 50-mL Teflon autoclave, into which a piece of CF was introduced. The autoclave was sealed and subjected to heat treatment at 120°C for 6 h in an oven. In the second step, the precursor material was fluorinated in a tube furnace under Ar gas protection.[1] Specifically, 1.5 g of NH_4F and the precursor were strategically positioned upstream and downstream of the heating zone in the furnace, respectively. The annealing process involved heating to 350°C at a controlled rate of 5°C·min^{-1}, maintaining this temperature for 2 h, and allowing it to cool naturally to room temperature.

Synthesis of electrodeposited Co(OH)$_2$ NS/CF: Electrodeposition was carried out in a 0.5 M $Co(NO_3)_2 \cdot 6H_2O$ aqueous solution adopting chronoamperometry at -1.0 V for 10 min. A piece of CF (0.5 cm × 1 cm), a SCE, and a Pt plate were used as the working electrode, reference electrode, and counter electrode, respectively.

Characterizations: XRD patterns were acquired using a Rigaku X-ray diffractometer

(Ultima IV, Japan) with Cu Kα radiation (40 kV, 30 mA). SEM images were captured using a ZEISS scanning electron microscope (Sigma 500, Germany). TEM images were obtained from a Thermo Fisher transmission electron microscope (Talos F200X, America). XPS spectra were recorded employing a Thermo ESCALAB 250Xi spectrometer (Scientific K-Alpha, America) with Al Kα radiation (12 kV, 6 mA). Absorbance spectra were measured using a Shimazu UV-vis spectrophotometer (UV-2600, Japan). In situ mass spectrometry was conducted on a Linglu mass spectrometer (QAS100, China). DEMS was conducted on a mass spectrometer (Linglu QAS100) to in situ analysis of produced intermediates and products. In situ Raman spectra were measured on a HORIBA confocal microscope (LabRAM HR Evolution, France) with a 532 nm laser. In situ attenuated total reflection fourier transform infrared spectroscopy (ATR-FTIR) spectra were recorded on a Thermo Fisher infrared spectrometer (Nicolet™ iS50, America).

Electrochemical measurements: The electrochemical performance of NO_3RR was evaluated on an electrochemical workstation (Chenhua CHI760E, Shanghai) using an H-type cell with three electrodes. Specifically, a piece of CoF_2 NS/CF (the area in contact with the electrolyte was 0.3 cm^2) was the working electrode. A Pt plate (1.0 cm^2) and a Hg/HgO electrode served as the counter and reference electrodes, respectively. The electrolyte was 0.1 M NaOH solution with or without 0.1 M NO_3^-. Initially, linear sweep voltammetry (LSV) was conducted over the potential window from −0.8 to −1.6 V vs. $E_{Hg/HgO}$ at a scan rate of 5 mV·s^{-1}. LSV was performed until the LSV curves exhibited negligible discrepancies. All recorded potentials were converted to the reversible hydrogen electrode (RHE) scale using the following equation: $E_{RHE} = E_{Hg/HgO} + 0.059pH + 0.097$. Chronoamperometry was then conducted at various potentials for 1 h to assess the rate of ammonia production and FE, which were determined as follows:

Yield = $C \times V / (A \times t)$,

FE = $n \times F \times C \times V / (M.R. \times Q)$,

where C, V, A, t, n, F, M.R., and Q are the product concentration in the catholyte, catholyte volume (30 mL), geometric area of the electrode (0.3 cm^2), time (1 h), electron transfer number, the Faraday constant (96485 C·mol^{-1}), relative molecular mass of the product, and applied potential, respectively.

DEMS was conducted using an Linglu in-situ mass spectrometer combined with a 760E electrochemical workstation. A small electrolytic cell with a volume of 2 mL was used, and the electrolyte was bubbled with high-purity Ar gas for 30 min to remove O$_2$ and N$_2$. The CoF$_2$ nanosheet (25 μg) was loaded on a planar conductive film (a dedicated film for in situ detection) to serve as the working electrode. A Pt wire and an Ag/AgCl electrode were used as the counter and reference electrodes, respectively. In situ mass spectrometry was performed simultaneously with chronoamperometry tests at different potentials (-0.1 ~ -0.6 Vvs. RHE). to detect products and intermediates.

Electrochemical in situ Raman experiments were carried out on a LabRAM HR spectrometer with 532 nm laser, a 50× objective, and an acquisition time of 90 s. In an in-house made Raman cell with , a piece of CoF$_2$ NS/CF, an Hg/HgO, and a Pt wire were used as the working electrode, reference electrode, and the counter electrode, respectively. Then the electrochemical tests using Amperometric i-t technique were performed at 0.1 ~ -0.6 V vs. RHE.

Electrochemical in situ ATR-FTIR tests were recorded on a Nicolet™ iS50 infrared spectrometer using internal reflection mode. The electrochemical experiments were tested in a Pike Veemax III ATR cell. The working electrode was prepared by loading CoF$_2$ nanosheets (25 μg) on a silicon wafer with Au coating. An Hg/HgO and a Pt wire were used as the reference electrode and the counter electrode, respectively. Amperometric i-t technique was applied at different potentials (OCP, -0.1 ~ -0.6 Vvs. RHE).
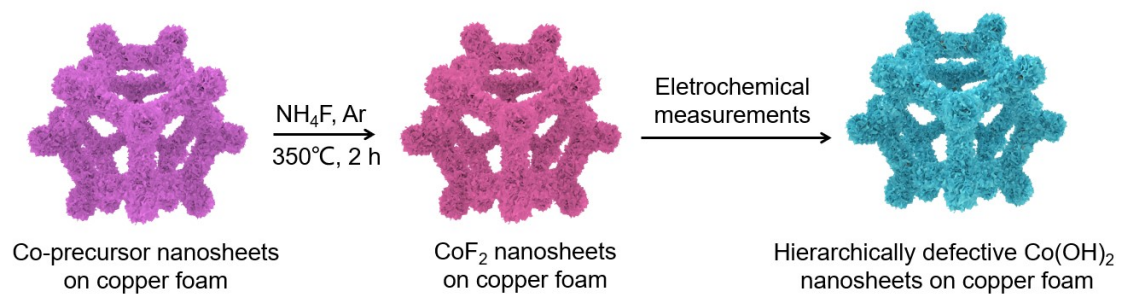
Determination of products: NH_3 in the catholyte was quantified using the indophenol blue method. Unless specified otherwise, the electrolyte was diluted by a factor of 50. The color agent was prepared by dissolving 5.0 g of salicylic acid and 5.0 g of sodium citrate in 100 mL of 1.0 M NaOH solution. The oxidizing agent was prepared by diluting 6.0 mL of NaClO (containing 5% available chlorine) to 100 mL in a volumetric flask. The catalyst solution was obtained by adding 0.1 g of $Na_2[Fe(CN)_5NO] \cdot 2H_2O$ to 10 mL of deionized water. Specifically, 2 mL of the color agent, 1 mL of the oxidizing agent, and 200 μL of the catalyst solution were sequentially added to 2 mL of the diluted catholyte. After incubating in the dark for 70 min, the ultraviolet–visible (UV–Vis) absorption spectra were measured in the wavelength range of 800–500 nm.

NO_2^- was quantified through spectrophotometry using the Griess method. The Griess reagent was formulated by dissolving 0.1 g of $C_{12}H_{14}N_2 \cdot 2HCl$, 1.0 g of sulfonamide, and 2.94 mL of H_3PO_4 in 50 mL of H_2O. Unless specified otherwise, the catholyte was diluted by a factor of 50. In a standard colorimetric assay, 1.0 mL of the diluted catholyte and 1.0 mL of the Griess reagent were added into 2.0 mL of H_2O. After a 10-min incubation period, the UV–Vis absorption spectra were measured in the wavelength range of 650–400 nm.

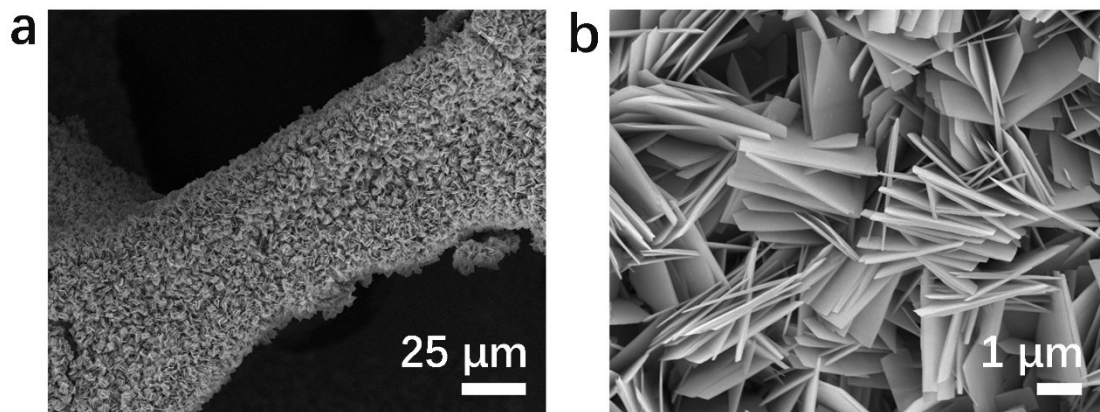N_2H_4 was also detected using a colorimetric method. The color agent was prepared by adding 1.99 g of p-C9H11NO (5.99 g) and 10 mL of HCl (37%) into 100 mL of C_2H_5OH. Thereafter, 2 mL of the undiluted catholyte was added to 2 mL of the color reagent. After 10 min, the UV–Vis absorption spectra were measured within the wavelength range of 500–400 nm.

DFT calculation methods: First-principles calculations with spin polarization were conducted using DFT, as implemented in the VASP package.[2] The projector-augmented wave method was used to model the interaction between valence electrons and ionic cores, and the cutoff energy was 450 eV.[3] The Perdew–Burke–Ernzerhof functional with DFT-D3 semi-empirical corrections was utilized to account for the
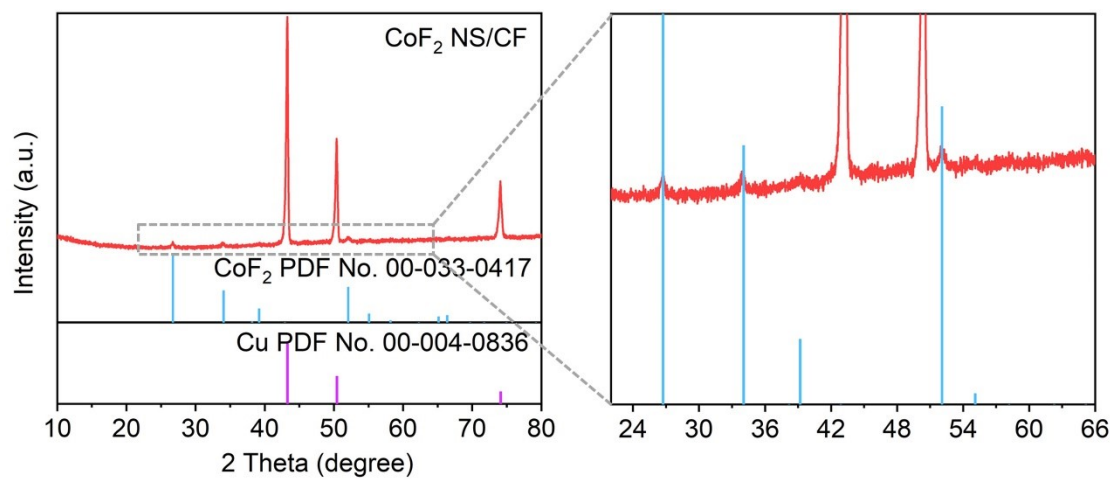
exchange-correlation effects within the framework of the generalized gradient approximation.[4] A Co(OH)$_2$(001) slab was constructed; the slab and its periodically repeated images were separated by a vacuum space of > 15 Å to prevent interactions along the z-direction. The Hubbard model was implemented with an effective on-site Coulomb interaction U of 3.52 eV for the Co *3d* orbital.[5] To optimize the structural configuration, the Brillouin zone was sampled using a 3 × 3 × 1 grid of special k-points, implemented through the Monkhorst–Pack scheme.[6] The convergence criteria for forces and total energy were set at 0.02 eV/Å and less than 1×10^{-5} eV, respectively.

Scheme 1. Illustration of the formation of Co(OH)$_2$ NS/CF.

Co-precursor nanosheets on copper foam

NH$_4$F, Ar
350℃, 2 h

CoF$_2$ nanosheets on copper foam

Eletrochemical measurements

Hierarchically defective Co(OH)$_2$ nanosheets on copper foam

Fig. S1 (a, b) SEM images of the Co-precursor nanosheets array on CF.

Fig. S2 XRD pattern of CoF$_2$ NS/CF.
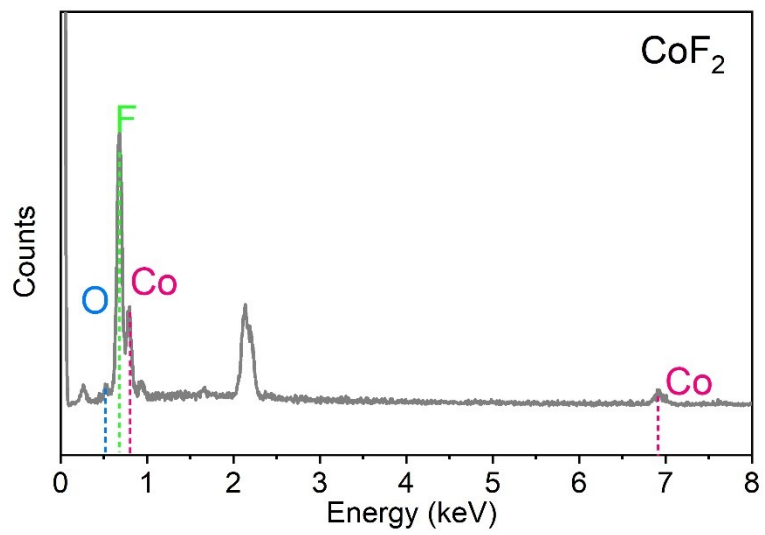
Fig. S3 EDX spectrum of CoF_2 NS/CF.
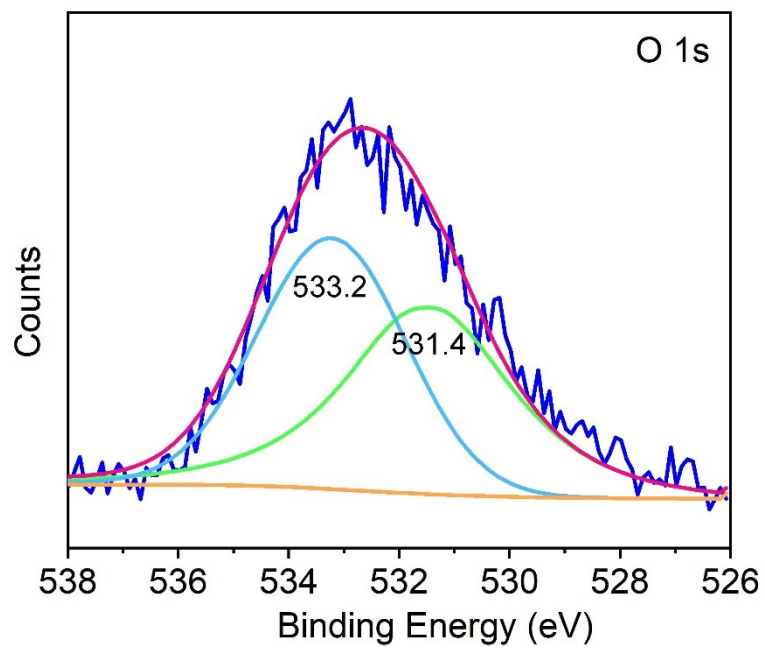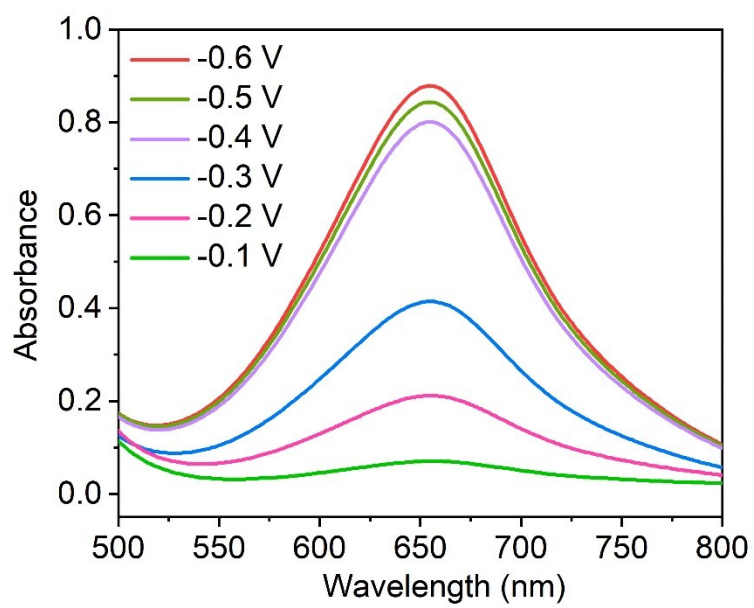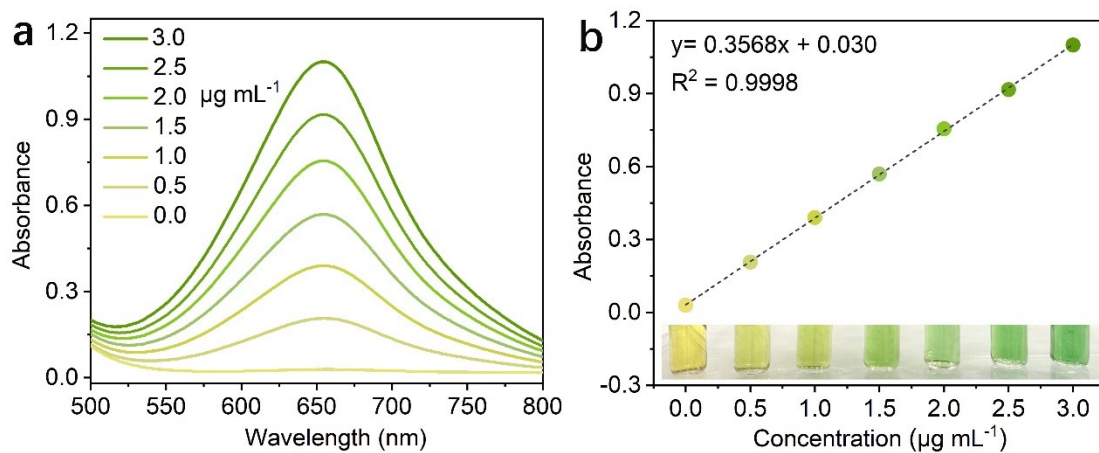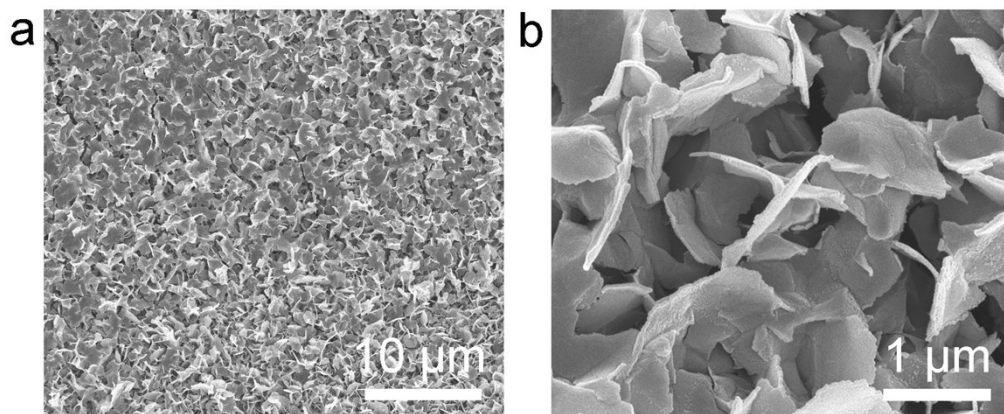
Fig. S4 XPS spectra of CoF_2 NS/CF in O 1s region of CoF_2 NS/CF.
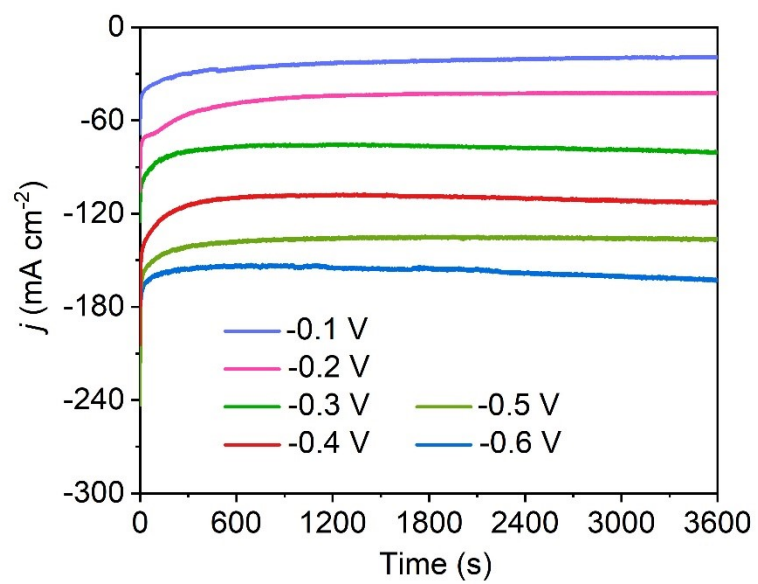
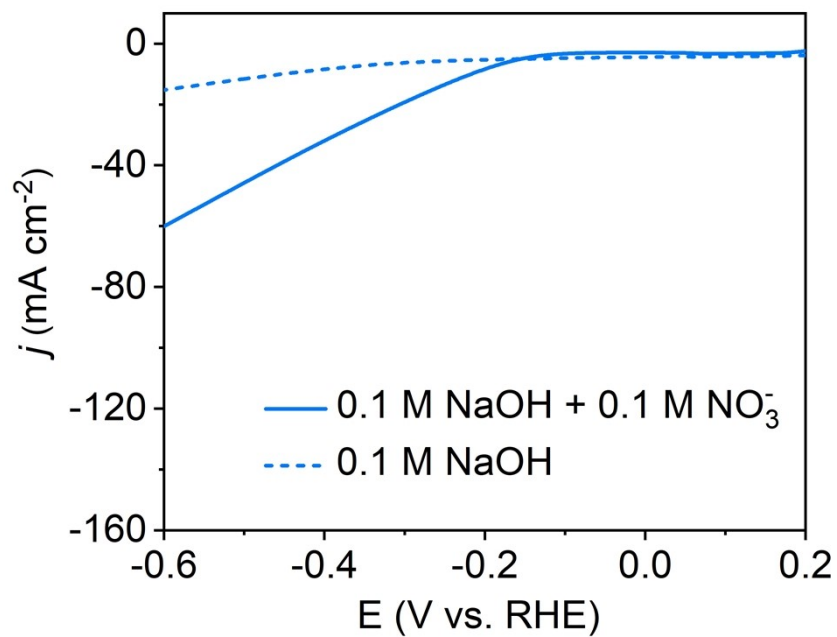**Fig. S5** Current density-time curves at various applied potentials of CoF$_2$ NS/CF.

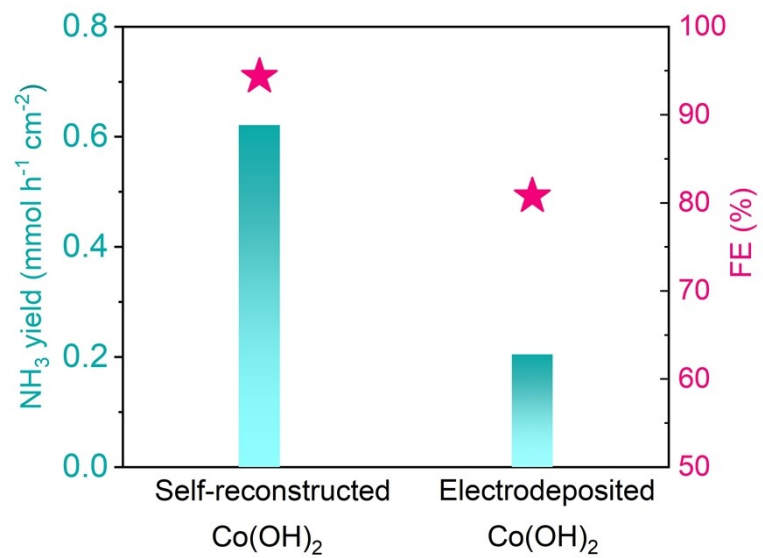**Fig. S6** UV-Vis absorption spectra for NH_3 detection at various applied potentials.

Fig. S7 (a) UV-Vis spectra of a series of solutions with known NH₃ concentration and (b) corresponding calibration curve.

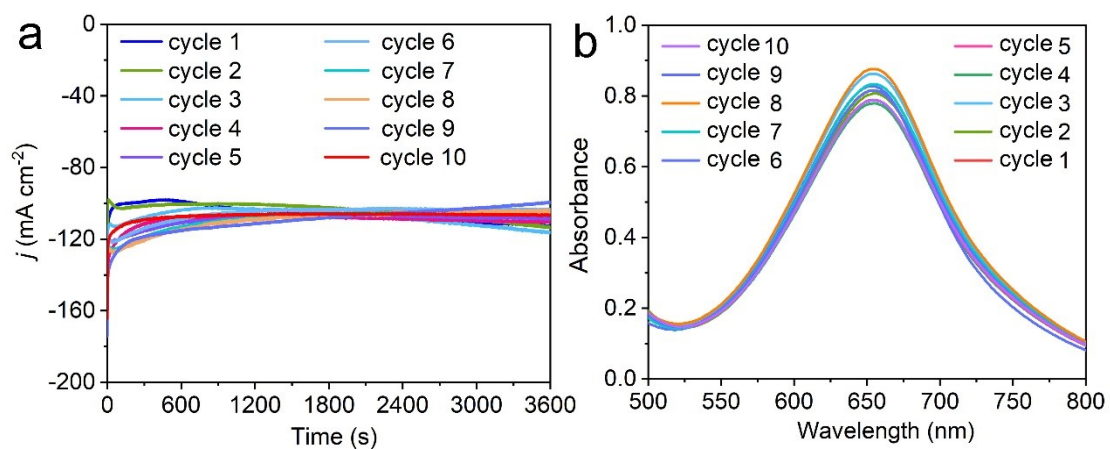**Fig. S8** (a,b) SEM images of electrodeposited Co(OH)$_2$ nanosheets on CF.

**Fig. S9** LSV curves of electrodeposited $Co(OH)_2$ NS/CF measured in NaOH with and without NO_3^-.

Fig. S10 NH$_3$ yields and FEs of self-reconstructed and electrodeposited Co(OH)$_2$ nanosheets on CF at -0.4 V.
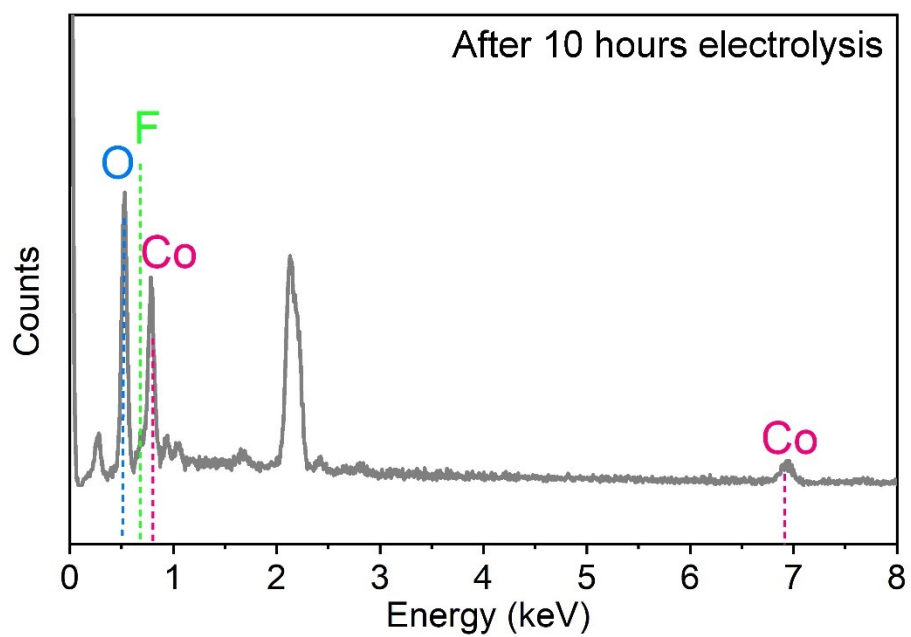
Fig. S11 (a) Chronoamperometry curves and (b) UV-Vis spectra of the catholytes stained with indophenol indicator for cycling tests.
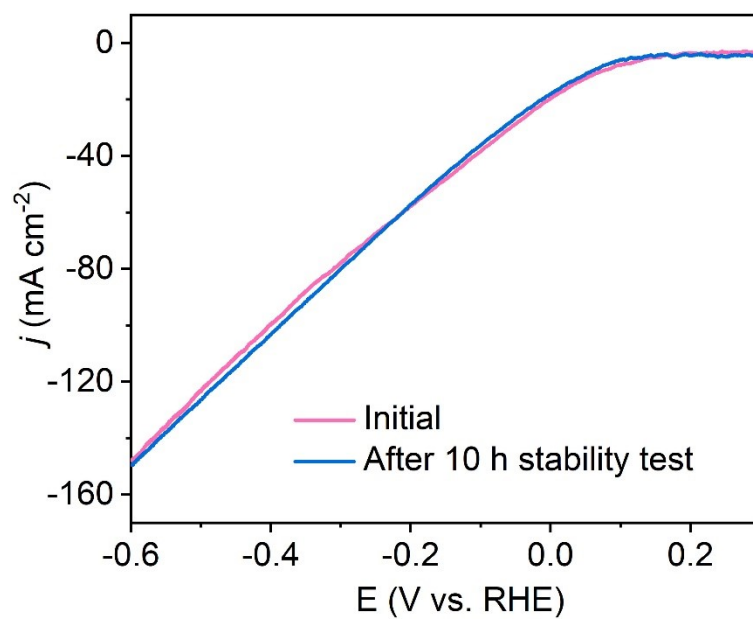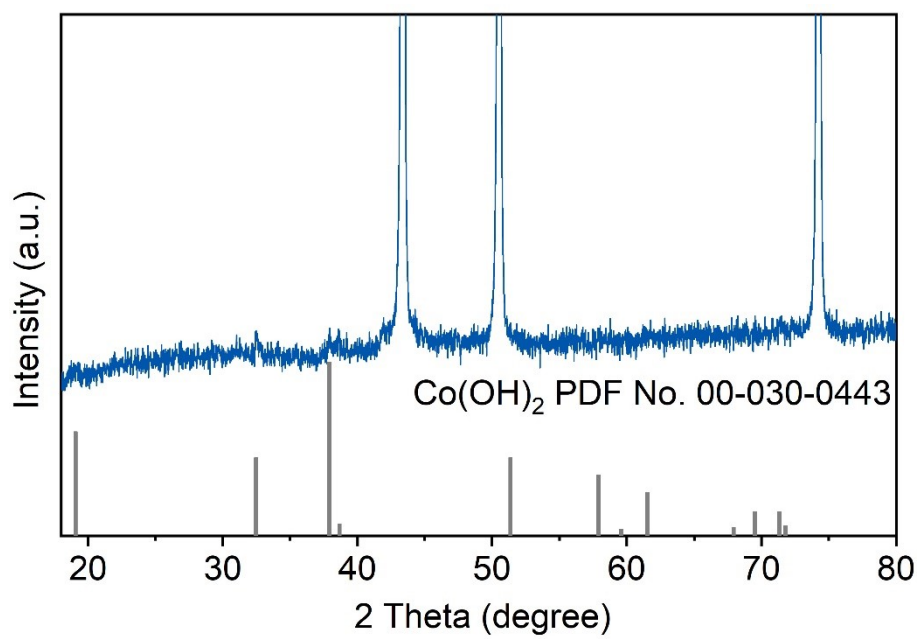
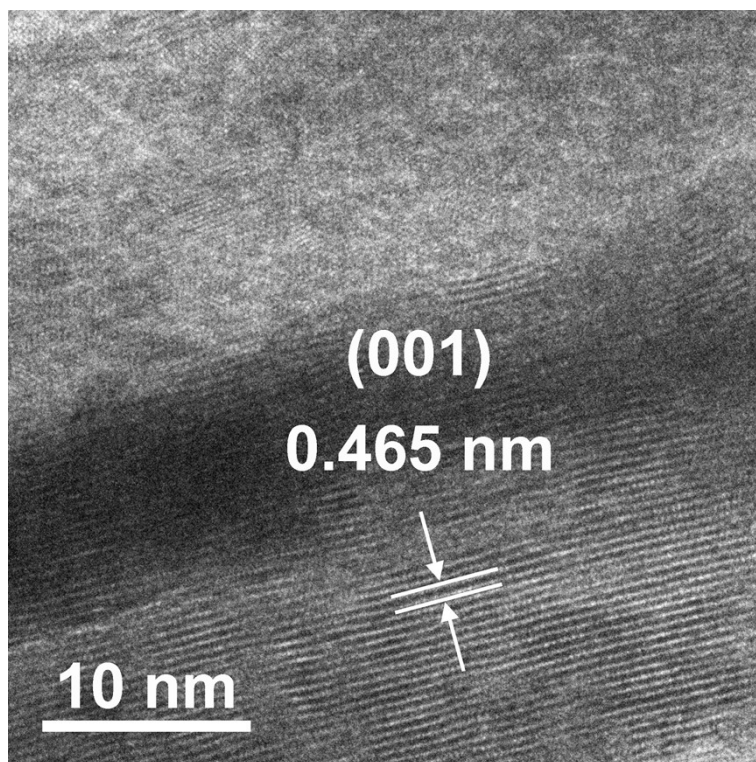**Fig. S12** LSV curves for CoF$_2$ NS/CF before and after 10 h consecutive recycling test.
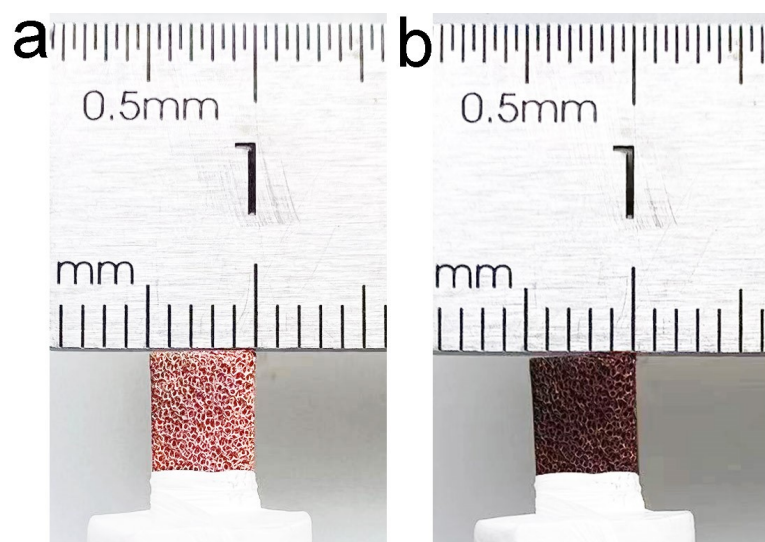
Fig. S13 Photographs of the working electrode (a) before and (b) after ENRA tests.

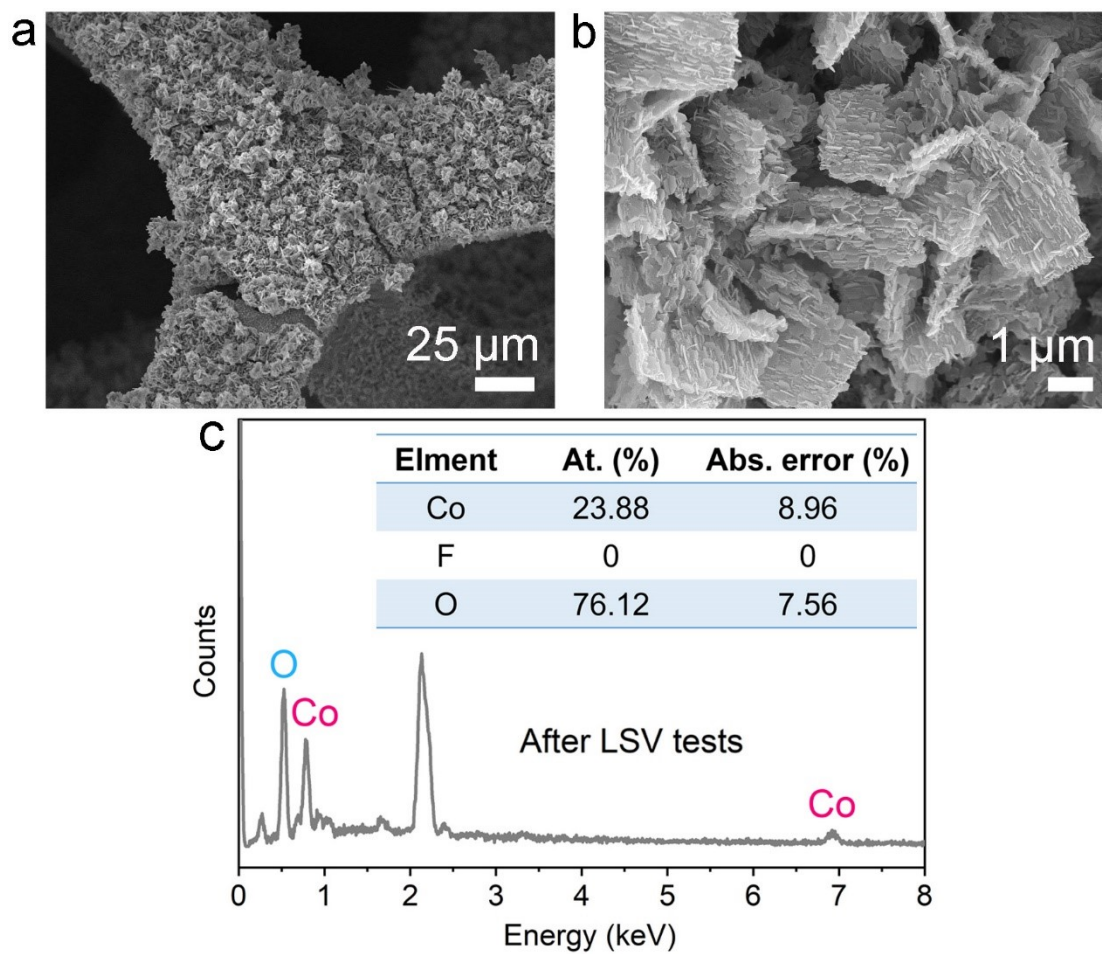**Fig. S14** EDX spectrum of CoF_2 NS/CF after 10 h electrolysis.

Co(OH)$_2$ PDF No. 00-030-0443
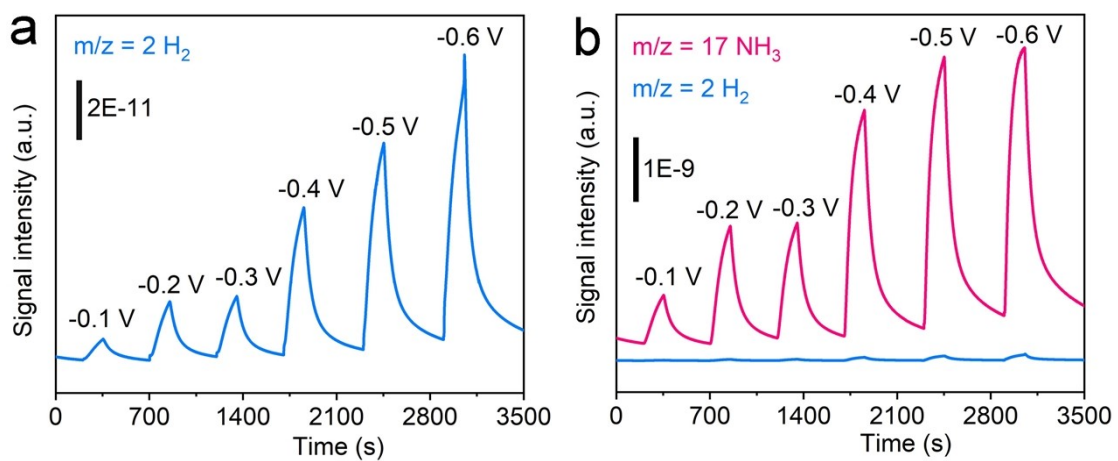
Fig. S15 XRD pattern of CoF$_2$ NS/CF post ENRA electrolysis.

Fig. S16 High-resolution TEM image of a vertical Co(OH)$_2$ nanosheet in Fig. 3c.

Element	At. (%)	Abs. error (%)
Co	23.88	8.96
F	0	0
O	76.12	7.56

After LSV tests

Fig. S17 (a, b) SEM images and (c) EDX spectrum of CoF_2 NS/CF after LSV tests.

Fig. S18 DEMS data (a) H_2 spectrum over $Co(OH)_2$ NS at different potentials; (b) H_2 and NH_3 spectra plotted in one graph for comparison.
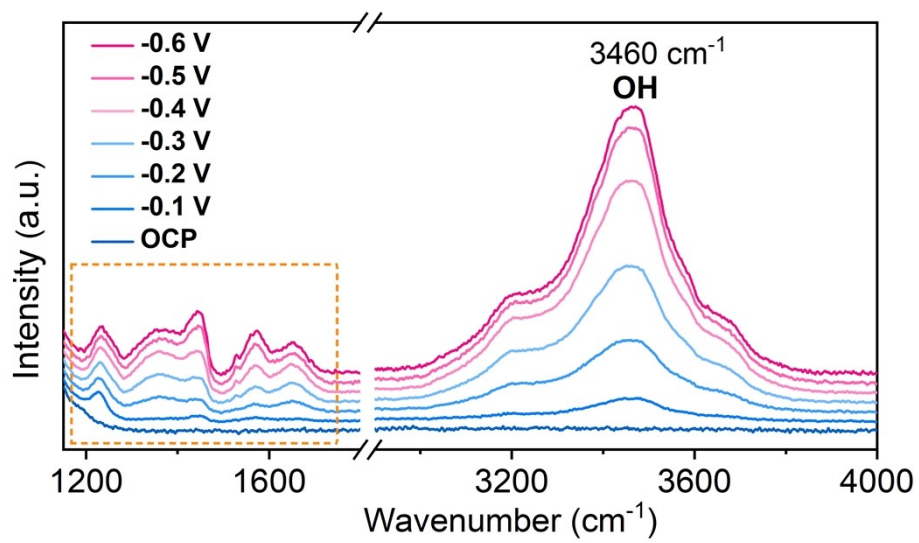
Fig. S19 In situ FTIR spectra of CoF$_2$ NS measured during ENRA tests.
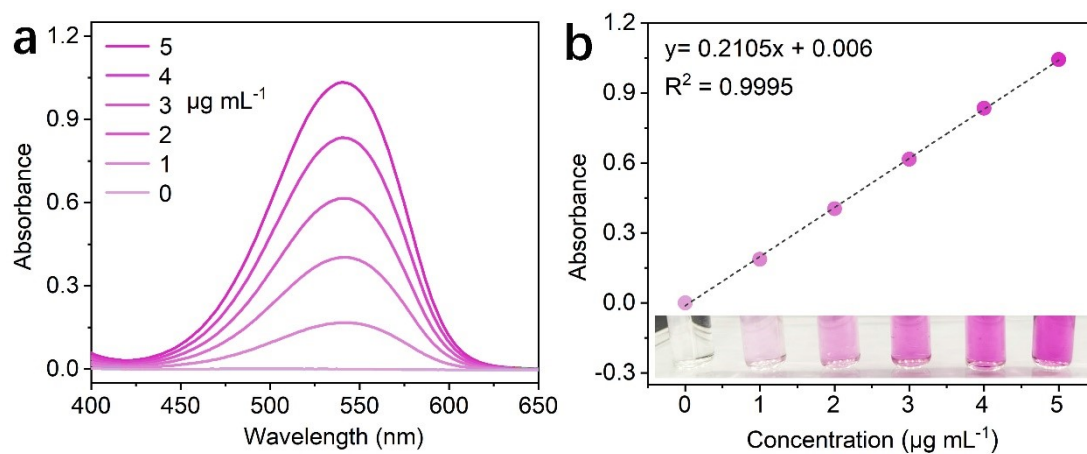
Fig. S20 (a) UV-Vis spectra of a series of solutions with known NO_2^- concentration and (b) corresponding calibration curve.
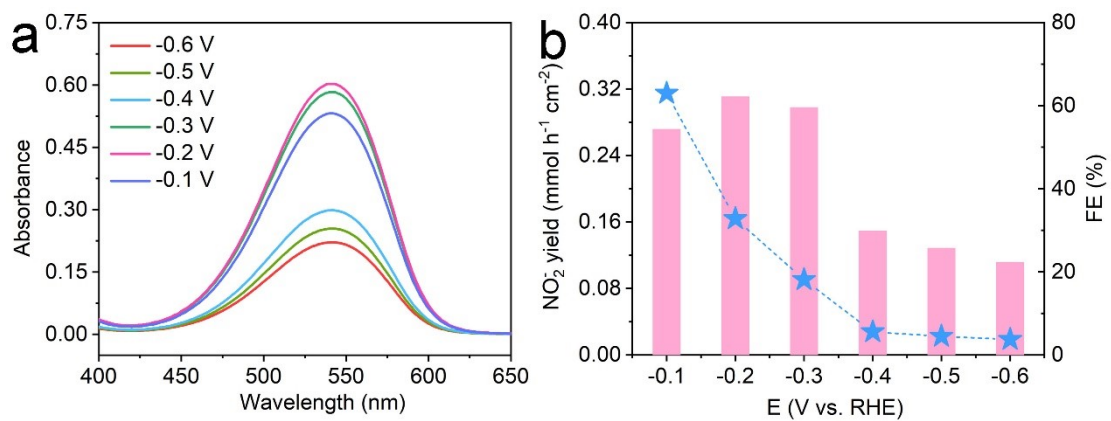
Fig. S21 (a) UV-Vis spectra of the diluted catholytes for NO_2^- detection at different applied potentials.
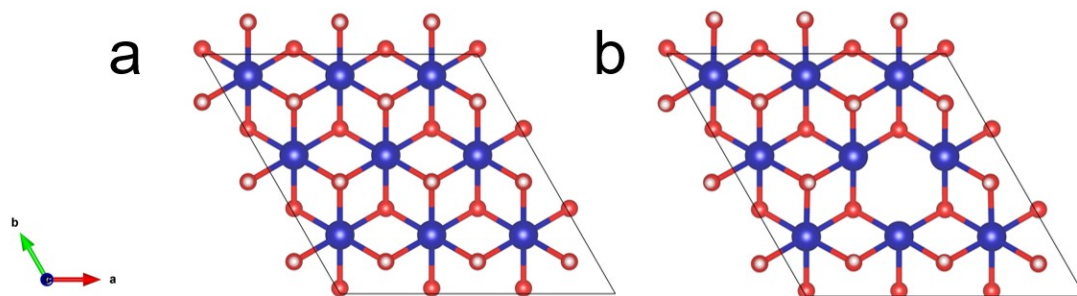
Fig. S22 Atomic structures of (a) $Co(OH)_2(001)$ and (b) defective $Co(OH)_2(001)$.
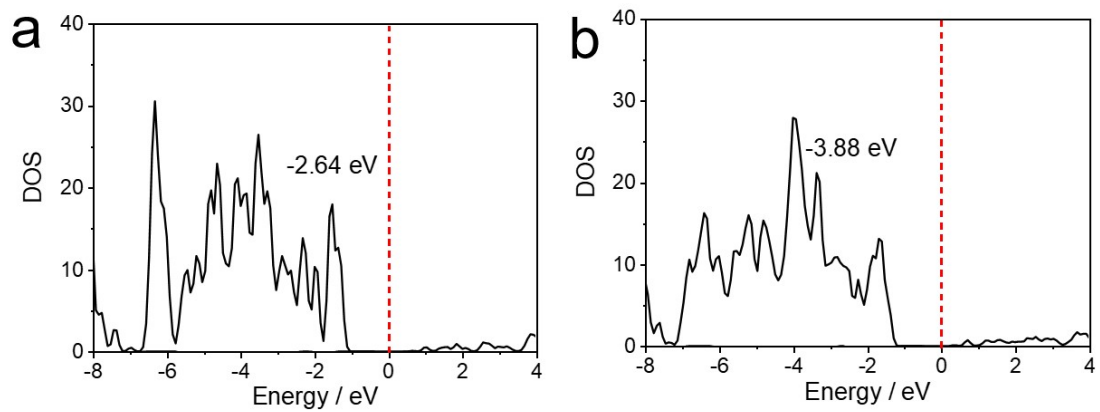
Fig. S23 DOS of (a) Co(OH)$_2$(001) and (b) defective Co(OH)$_2$(001).

Fig. S24 Adsorption free energies of *NO$_3$ and *H on Co(OH)$_2$ (001) and the corresponding atomic structures.

Table S1 ENRA performance comparison of Co(OH)$_2$ NS/CF with other reported Co-based electrocatalysts.

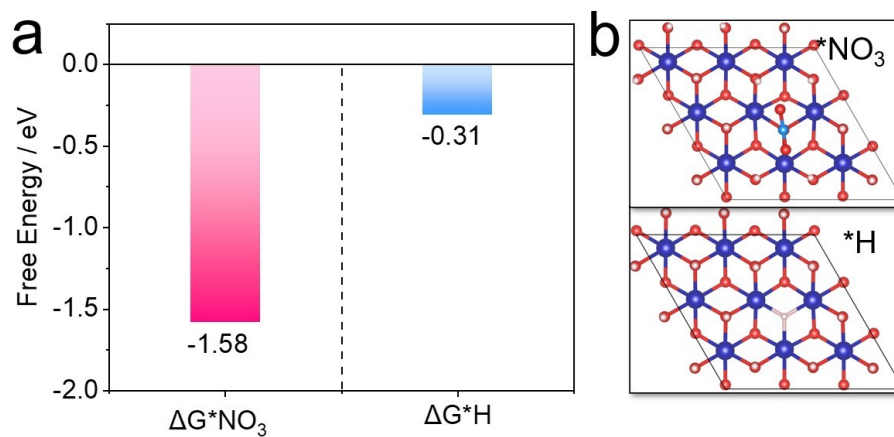| Catalyst	Electrolyte	Potential (V vs. RHE)	NH$_3$ yield (mmol h^{-1} cm^{-2})	FE	Ref.
Self-reconstructed Co(OH)$_2$	0.1 M NaOH 0.1 M NaNO$_3$	-0.4	0.62	94.3	This work
Electrodeposited Co(OH)$_2$	0.1 M NaOH 0.1 M NaNO$_3$	-0.4	0.20	80.7	This work
Y–Co(OH)F	0.5 M K$_2$SO$_4$ 200 mg L^{-1} KNO$_3$	-1.3 (vs. SCE)	0.2149	91.81	[7]
CoFe LDH	1.0 M KOH 1400 ppm KNO$_3$	-0.45	0.93	97.68	[8]
Co(OH)$_2$ (prepared by hydrothermal method)	1.0 M KOH 1400 ppm KNO$_3$	-0.45	–	85.86	[8]
Co@CC	0.1 M NaOH 0.1 M NaNO$_3$	-0.8	0.60	93.4	[9]
CoNPs/CF	1.0 M KOH 0.1 M KNO$_3$	-0.2	~0.20	92	[10]
Co/CoO	0.1 M PBS 500 ppm KNO$_3^-$	-0.65	0.2	93.8	[11]
CoOx	0.1 M KOH 0.1 M NO$_3^-$	-0.3	0.33	93.4	[12]
NiCo$_2$O$_4$	0.1 M NaOH 0.1 M NaNO$_3$	-0.3	0.468	99.0	[13]

$CoAl_2O_4$	0.1 M PBS 0.1 M KNO_3	-0.7	~0.36	92.6	[14]
$FeCo_2O_4$	1.0 M KOH 20 mM KNO_3	-0.5	~0.293	95.9	[15]
Reduced Co_3O_4	0.1 M K_2SO_4 200 ppm NO_3	-0.05	7.25 (mg h^{-1} $mg_{cat.}^{-1}$)	74.8	[16]
Co_2B/BCN	0.1 M KOH 0.1 M KNO_3	-0.5	5.73 (mg h^{-1} $mg_{cat.}^{-1}$)	96.61	[17]
CoP/TiO_2	0.1 M NaOH 0.1 M $NaNO_3$	-0.3	0.4998	95	[18]
$Fe-CoS_2$	0.5 M Na_2SO_4 0.1 M $NaNO_3$	-0.6	0.63	97.5	[19]
CoS_2	0.5 M Na_2SO_4 0.1 M $NaNO_3$	-0.6	0.23	67.38	[19]
Co-doped Fe/Fe_2O_3	0.1 M Na_2SO_4 0.036 M $NaNO_3$	-0.75	~0.088	85.2	[20]

References

1. Q. Dong, T. Su, W. Ge, Y. Ren, Y. Liu, W. Wang, Q. Wang and X. Dong, Atomic doping and anion reconstructed CoF_2 electrocatalyst for oxygen evolution reaction, *Adv. Mater. Interfaces*, 2020, **7**, 1901939.

2. H. J. Kresse G, Ab initio molecular-dynamics simulation of the liquid-metal-amorphous-semiconductor transition in germanium, *Phys. Rev. B*, 1994, **49**, 14251−14269.

3. G. Kresse and D. P. Joubert, From ultrasoft pseudopotentials to the projector augmented-wave method, *Phys. Rev. B*, 1999, **59**, 1758−1775.

4. B. K. Perdew JP, Ernzerhof M., Generalized gradient approximation made simple, *Phys. Rev. Lett.*, 1996, **18**, 3865−3868.

5. H. Jin, S. Mao, G. Zhan, F. Xu, X. Bao and Y. Wang, Fe incorporated α-Co(OH)$_2$ nanosheets with remarkably improved activity towards the oxygen evolution reaction, *Phys. Rev. B*, 2017, **5**, 1078−1084.

6. H. J. Monkhorst and J. D. Pack, Special points for Brillouin-zone integrations, *Phys. Rev. B*, 1976, **13**, 5188−5192.

7. Z. Yu, T. Ren, J. Xie, H. Yu, K. Deng, Z. Wang, H. Wang, L. Wang and Y. Xu, Yttrium atomically incorporated into Co(OH)F nanowires enables efficient electrochemical reduction of nitrate to ammonia, *Chem. Commun.*, 2023, **59**, 13875−13878.

8. F. Du, J. Li, C. Wang, J. Yao, Z. Tan, Z. Yao, C. Li and C. Guo, Active sites-rich layered double hydroxide for nitrate-to-ammonia production with high selectivity and stability, *Chem. Eng. J,* 2022, **434**, 134641.

9. T. Xie, X. Li, J. Li, J. Chen, S. Sun, Y. Luo, Q. Liu, D. Zhao, C. Xu, L. Xie and X. Sun, Co nanoparticles decorated corncob-derived biomass carbon as an efficient electrocatalyst for nitrate reduction to ammonia, *Inorg. Chem.*, 2022, **61**, 14195−14200.

10. Y. Qian, J. Lv, Y. Zhong, X. Liu, X. Li, Y. Peng, J. Yan and A. Wu, Efficient electrocatalytic nitrate reduction using 3D copper foam-supported Co hexagonal nanoparticles in a membrane electrode assembly, *Int. J. Hydrogen Energy,* 2024, **64**, 178−185.

11. Y. Yu, C. Wang, Y. Yu, Y. Wang and B. Zhang, Promoting selective electroreduction of nitrates to ammonia over electron-deficient Co modulated by rectifying Schottky contacts, *Sci. China Chem.*, 2020, **63**, 1469-1476.

12. J. Wang, C. Cai, Y. Wang, X. Yang, D. Wu, Y. Zhu, M. Li, M. Gu and M. Shao, Electrocatalytic reduction of nitrate to ammonia on low-cost ultrathin CoOx nanosheets, *ACS Catal.*, 2021, **11**, 15135−15140.

13. Q. Liu, L. Xie, J. Liang, Y. Ren, Y. Wang, L. Zhang, L. Yue, T. Li, Y. Luo, N. Li, B. Tang, Y. Liu, S. Gao, A. A. Alshehri, I. Shakir, P. O. Agboola, Q. Kong, Q.

Wang, D. Ma and X. Sun, Ambient ammonia synthesis via electrochemical reduction of nitrate enabled by $NiCo_2O_4$ nanowire array, *Small*, 2022, **18**, 2106961.

14. Z. Deng, J. Liang, Q. Liu, C. Ma, L. Xie, L. Yue, Y. Ren, T. Li, Y. Luo, N. Li, B. Tang, A. Ali Alshehri, I. Shakir, P. O. Agboola, S. Yan, B. Zheng, J. Du, Q. Kong and X. Sun, High-efficiency ammonia electrosynthesis on self-supported Co_2AlO_4 nanoarray in neutral media by selective reduction of nitrate, *Chem. Eng. J.*, 2022, **435**, 135104.

15. J. Li, D. Zhao, L. Zhang, L. Yue, Y. Luo, Q. Liu, N. Li, A. A. Alshehri, M. S. Hamdy, Q. Li and X. Sun, A $FeCo_2O_4$ nanowire array enabled electrochemical nitrate conversion to ammonia, *Chem. Commun.,* 2022, **58**, 4480-4483.

16. D. Lu, T. Liu, J. Han, J. Zhao and H. Wang, Yolk-shell composite oxides with binuclear Co(II) sites toward low-overpotential nitrate reduction to ammonia, *Chem. Eng. J.*, 2023, **477**, 146896.

17. L. Hu, D. Zhao, C. Liu, Y. Liang, D. Zheng, S. Sun, Q. Li, Q. Liu, Y. Luo, Y. Liao, L. Xie and X. Sun, Amorphous CoB nanoarray as a high-efficiency electrocatalyst for nitrite reduction to ammonia, *Inorg. Chem. Front.,* 2022, **9**, 6075−6079.

18. Z. Deng, C. Ma, X. Fan, Z. Li, Y. Luo, S. Sun, D. Zheng, Q. Liu, J. Du, Q. Lu, B. Zheng and X. Sun, Construction of CoP/TiO_2 nanoarray for enhanced electrochemical nitrate reduction to ammonia, *Mater. Today Phy.*, 2022, **28**, 100854.

19. N. Zhang, G. Wang, G. Zhang, K. Chen and K. Chu, Electrochemical nitrate-to-ammonia reduction over atomic Fe-dopants incorporated in CoS_2, *Chem. Eng. J.*, 2023, **474**, 145861.

20. S. Zhang, M. Li, J. Li, Q. Song and X. Liu, High-ammonia selective metal organic framework derived Co-doped Fe/Fe_2O_3 catalysts for electrochemical nitrate reduction, *PNAS*, 2022, **119**, e2115504119.